

Animation and Chirplet-Based Development of a PIR Sensor Array for Intruder Classification in an Outdoor Environment

Raviteja Upadrashta, Tarun Choubisa, A. Praneeth, Tony G., V. S. Aswath, P. Vijay Kumar, Fellow, IEEE
 Dept. of Electrical Comm. Engg., Indian Institute of Science, Bengaluru, 560012, India
 Sripad Kowshik, Hari Prasad Gokul R, T. V. Prabhakar
 Dept. of Electronic Systems Engg., Indian Institute of Science, Bengaluru, 560012, India

Abstract—This paper presents the development of a passive infra-red sensor tower platform along with a classification algorithm to distinguish between human intrusion, animal intrusion and clutter arising from wind-blown vegetative movement in an outdoor environment. The research was aimed at exploring the potential use of wireless sensor networks as an early-warning system to help mitigate human-wildlife conflicts occurring at the edge of a forest. There are three important features to the development. Firstly, the sensor platform employs multiple sensors arranged in the form of a two-dimensional array to give it a key spatial-resolution capability that aids in classification. Secondly, given the challenges of collecting data involving animal intrusion, an Animation-based Simulation tool for Passive Infra-Red sEnsor (ASPIRE) was developed that simulates signals corresponding to human and animal intrusion and some limited models of vegetative clutter. This speeded up the process of algorithm development by allowing us to test different hypotheses in a time-efficient manner. Finally, a chirplet-based model for intruder signal was developed that significantly helped boost classification accuracy despite drawing data from a smaller number of sensors. An SVM-based classifier was used which made use of chirplet, energy and signal cross-correlation-based features. The average accuracy obtained for intruder detection and classification on real-world and simulated data sets was in excess of 97%.

Index Terms—Wireless sensor network, passive infra-red sensor, intrusion detection, chirplets, animation, wildlife protection.

I. INTRODUCTION

As described above, this project¹ concerns the development of a Passive Infra-Red (PIR) based Sensor Tower Platform

¹The work presented here was supported in part by an Indo-US project jointly funded by the US National Science Foundation and the Indian Department of Electronics and Information Technology.

(STP) that can distinguish between humans, animals and wind-blown vegetative clutter in an outdoor setting. We limit our attention to a small subclass of animals that are comparable in size and shape to a tiger or a dog. In the sequel², we will refer to this sub-class of animals simply as animals. Also, when we speak of an intruder, the intruder could be either human or animal. We will refer to clutter generated by wind-blown vegetation as simply clutter. Power is not commonly available in settings of the type considered here and this motivates the use of low-power sensor networks.

A. Prior Work

PIR sensors for detecting human motion in outdoor environments has only recently been investigated [1]–[5]. Hong et. al. in [4] use digital PIR sensors and energy thresholding for detecting human motion. The amount of signal processing that can be done using digital PIR sensors is limited in comparison to analog sensors that allow more sophisticated signal-processing algorithms to be employed for rejecting clutter. In [2], the PIR signal is first high-pass filtered to remove low frequency components resulting from slow environment changes and the signal energy is then compared against an adaptive threshold. In [3], clutter signals arising from environmental changes and wind-blown vegetation are rejected by a Support Vector Machine (SVM) based classifier that uses a Haar transform-based feature vector. However, the articles [1]–[4] described above, do not consider the problem of distinguishing between human and animal intrusions.

²An earlier version of this paper was presented at the ISSNIP-2015 Conference. DOI:10.1109/ISSNIP.2015.7106914

The authors of [5] develop a Sensor Platform (SP) that is capable of classifying between human and animal that makes use of relatively expensive germanium lenses along with high resolution PIR sensors. The focus of the work presented here is on the development of a STP that makes use of off-the-shelf, relatively inexpensive PIR sensors and lenses. In a publication that appeared after the appearance of our 2015 conference publication [6], Zhao et. al. in [7] investigated the problem of discriminating between humans and false alarms generated by motion of animals of shape similar to dogs and geese using a single PIR sensor in conjunction with a multi-lens. However, false alarms potentially arising from moving vegetative clutter are not treated in this paper.

Section II provides background on the PIR sensor. Section III gives a detailed description of our approach to PIR STP design. Section IV describes our data collection efforts. Section V, provides a description of ASPIRE, an animation-based simulation tool that was used to simulate PIR signals generated by human and animal intrusions. Chirp-based modeling of the intruder signal and its use in classification is covered in Section VI. Other features employed for detection and classification are described in Section VII. Our classification algorithm and experimental results are presented in Section VIII. The final section draw conclusions and presents thoughts on future extensions of this work.

II. PIR SENSOR BACKGROUND

PIR sensors work on the principle of pyroelectricity which causes them to respond to changes in incident radiation [8]. This ability has been used in a wide range of applications such as temperature sensing, traffic control, fire alarms, thermal imaging, and radiometers [9]. A further application involves the detection of humans as there are estimates that place the heat radiated by a human up to as much as 100 W. The use of PIR sensors in detecting human motion has been restricted mainly to indoor applications ranging from home security, smart homes, health care, hallway monitoring, gesture recognition, walker recognition, etc. As noted below in Section II-C, there are challenges to be overcome when attempting to employ a PIR in an outdoor environment.

A. Block Diagram of a PIR Sensor

The block diagram of a typical, commercially-available PIR sensor is shown in Fig. 1. The PIR sensor typically consists

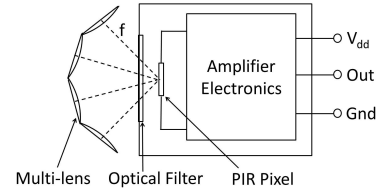


Fig. 1. The block diagram of a typical PIR sensor.

of several radiation-sensing elements, called pixels, arranged in the form of an array, a common form being a (1×2) arrangement as shown in Fig. 2(a). We will refer to this (1×2) PIR sensor, simply as a PIR sensor. The pair of pixels in the (1×2) arrangement are wired together in a differential manner to overcome false alarms triggered by changes in the ambient temperature. A lens system is typically used to expand the Field of View (FoV) of the sensor and plays a key role in defining the sensor output signal. The lens system serves to focus radiation from different directions onto the pixels and consists of either a single lens or a multi-lens. A multi-lens is a set of contiguous lenses sharing a common focal point. The multi-lens shown in Fig. 1 corresponds to a set of contiguous plano-convex lenses³. The FoV of the sensor can be viewed as a set of virtual beams cast out into space along which radiation is received. Fig. 2(a) illustrates the virtual beams cast out by a single spot lens, when placed in front of a (1×2) sensor. Given any plane in 3-dimensional space, the intersection of the FoV of the sensor with the plane is called the Virtual Pixel Array (VPA) associated with the particular plane. Fig. 2(a) shows the VPA associated to the (1×2) sensor used in conjunction with a spot lens. A typical signal generated as a result of a human intruder moving across the FoV of (1×2) PIR pixel array is shown in Fig. 2(b). When the spot lens is replaced by a multi-lens, the resulting virtual beams are shown in Fig. 2(c). The output of the sensor in this case is the superposition of the signals generated by each pair of virtual pixels. A typical signal output for such an arrangement is shown in Fig. 2(d).

The human being radiates the peak emission at a wavelength of roughly $10 \mu\text{m}$. An optical filter is used to reduce the influence of moving objects radiating at wavelengths significantly different from those of a human being.

³In practice, each plano-convex lens is replaced by a Fresnel lens to reduce attenuation of the incident radiation.

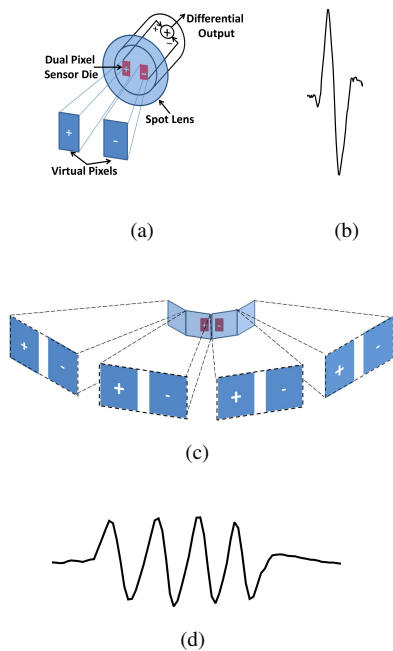


Fig. 2. The VPA associated with a (1×2) -pixel array and a spot lens is shown in (a). The corresponding signal generated when an intruder moves in a plane parallel to the face of the sensor is shown in (b). When the spot lens is replaced by a multi-lens, we obtain the VPA shown in (c) and the signal waveform displayed in (d).

B. PIR Signal Generation

1) *Radiation Model*: The first step in determining the signal generated by a PIR sensor is to estimate the net radiation received from the source. Assuming the source can be modelled as a Lambertian source, i.e., a source that radiates equal energy in all directions, the net power transfer is [10]

$$w(t) = \frac{\tau \eta F A_e A_{\text{proj}}(t) \sigma (T_{\text{obj}}^4 - T_{\text{b}}^4)}{\pi R^2}, \quad (1)$$

where, τ captures attenuation due to the atmosphere, η is the transmission coefficient of the lens, F is the fraction of the total radiation within the bandwidth of the optical filter, A_e is the area of the lens aperture, $A_{\text{proj}}(t)$ is the area of the source when projected on to the VPA, σ is the Stefan-Boltzmann's constant, T_{obj} is the object temperature in Kelvin, T_{b} is the background temperature in Kelvin and R is the distance of the radiating source from the detector.

2) *Impulse Response*: One can model a PIR sensor as a bandpass filter with an impulse response given by [11], [12]

$$h(t) = k_1 e^{-k_2 t} - k_3 e^{-k_4 t}, \quad (2)$$

where, the constants k_1 through k_4 depend on the physical properties of the PIR crystal and the amplifier electronics. The output voltage $v(t)$ of the PIR sensor in response to a time-varying incident input radiation $w(t)$ can be computed by simply convolving $w(t)$ with $h(t)$ i.e., $v(t) = w(t) * h(t)$.

Equation (1) and the above model of a PIR sensor are employed by ASPIRE to simulate the output signal of a PIR sensor as will be seen in Section V. Simulation of the signal is useful when we wish to quickly understand the efficacy of a particular lens design without expending the time and effort needed for real-world data collection.

C. Challenges Faced in an Outdoor Deployment of a PIR Sensor

One of the challenges to be overcome in an outdoor setting is the need to detect and classify in the presence of clutter. In such a setting, the radiation incident on a PIR could be altered due to changes in the environment, for example, when leaves blow in the wind or the sun comes out from behind a cloud.

III. APPROACH TO PIR SENSOR PLATFORM DESIGN

Our two principal objectives are rejecting false alarms arising from moving vegetation and distinguishing between human and animal intruder motion. Two simple observations were key to the development of the STP. Firstly, that it is possible to distinguish between human and animal based on their height. Secondly, intruder motion is translational in nature, while vegetative motion tends to be oscillatory.

The following assumptions were made:

- 1) At any given time, only a single intruder will be present within the FoV of the sensor;
- 2) Intruders move in a straight line at a uniform speed that is in a specified range: 1 to 3 m/sec;
- 3) Only animals having the same physical features as either a dog, wolf, leopard or tiger are considered here.

A. VPA Design

The sensor platform consists of an array of 8 sensors arranged in the form of a tower (and hence referred to as sensor tower platform), which are labelled as $A, B, C, D, L_1, L_2, R_1, R_2$ (see Fig. 3(a)). Sensors A, B, C and D are arranged as a vertical array (see Fig. 3(a)) to provide the spatial resolution needed to distinguish between human and animal based on their height. Sensors A, B share a common multi-lens (called multi-lens AB) as do sensors C, D (multi-lens CD). The VPA associated with sensors A, B, C, D is shown in Fig. 3(b).

Sensors L_1, L_2, R_1, R_2 are placed so as to form two vertical arrays (see Fig. 3(a)) to distinguish between translational and oscillatory motion. Sensors L_1, L_2 share a single spot lens L as do sensors R_1, R_2 (spot lens R). The VPA associated with sensors $L_i, R_i, i = 1, 2$, is shown in Fig. 3(b). If the intruder motion is translatory in nature with motion taking place from left to right of the STP, then the signal seen by sensor R_i will in general be a delayed version of the signal seen by L_i . This will not be the case with oscillatory motion in general and it is this feature that we exploit in distinguishing between intruder and clutter.

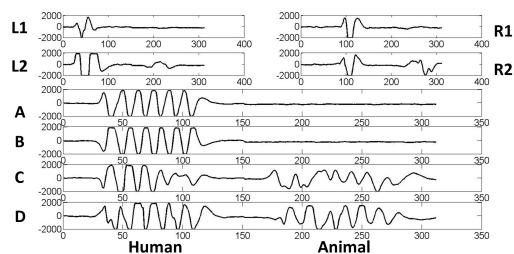
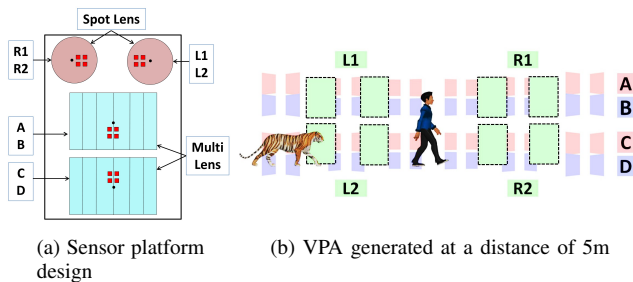


Fig. 3. Illustrating the VPA design and typical associated signals for a human and animal motion.

The sensors and amplifier electronics are housed inside an IP65 box. The lens mounts for the multi-lenses AB and CD were made using a 3D printer. A snapshot of the developed STP appears in Fig. 4. For additional detail relating to components used⁴, please see Table I.

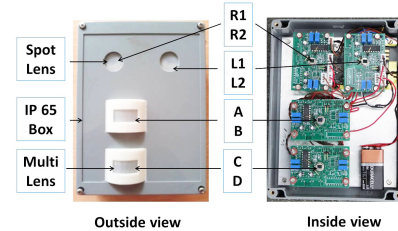


Fig. 4. The STP developed and its associated electronics.

TABLE I
SENSORS AND LENSES EMPLOYED IN EACH STP.

Component	Quantity	Company	Part No.
PIR Sensor	4	Nippon Ceramic	REP05B
Multi Lens	2	Kube Electronics	TR426
Spot Lens	2	Kube Electronics	TR1004

B. Use of Vertical Offset to Avoid Overlap Between Rows of the VPA

The need for making the STP as compact as possible, forces the close placement of the multi-lenses AB and CD . However, close placement of the two multi-lenses will cause rows B and C of the VPA to overlap at larger distances from the STP, leading to a loss in spatial resolution. To overcome this, we resorted to the simple but effective trick of vertically offsetting sensors A, B and C, D , i.e., placing sensors A, B slightly below the optical axis of multi-lens AB and sensors C, D slightly above the optical axis of multi-lens CD . This is illustrated in Fig. 5.

C. Electronics for Sensor Platform

The output of the PIR sensor is weak (typically on the order of μV) and needs amplification. A two-stage amplifier circuit is used to boost the signal amplitude (shown in Fig. 6). Potentiometers are used as feedback resistors at

⁴The REP05B PIR sensor package has its pixels arranged in a 2×2 fashion. The sensor provides two outputs, one for each row of differentially wired pixels.

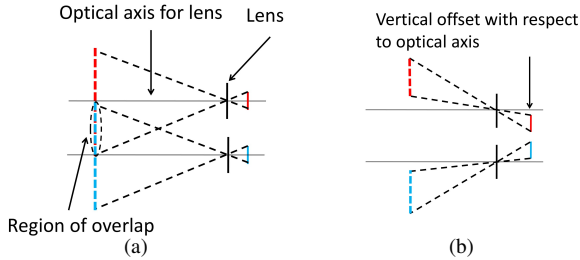


Fig. 5. In (a), it is shown that close spacing of two lenses (equivalently, multi-lenses) with sensors centered on the optical axes of the two lenses causes beams to overlap at a distance. This is prevented by the simple arrangement of sensors in (b), where the sensors are vertically offset with respect to the optical axes of the corresponding lenses.

each amplifier stage to provide a variable gain. The gain is adjusted in order to maintain a signal with large amplitude but free from saturation. The reason for this is that the signal processing techniques we employ for discriminating between various classes, is dependent on variations in signal amplitude. In order to improve the dynamic range of the amplifier, we provide a dual supply to the amplifier. This necessitates the inclusion of a rail-splitter. The rail-splitter takes the conventional single rail from a 9 V DC supply and splits it to provide a ± 4.5 V supply to the amplifiers. The output of the final amplification stage is DC level shifted by using a pull-up resistor in order to make the polarity of the signal positive (as the analog to digital converter on the mote requires signal inputs with a positive polarity only).

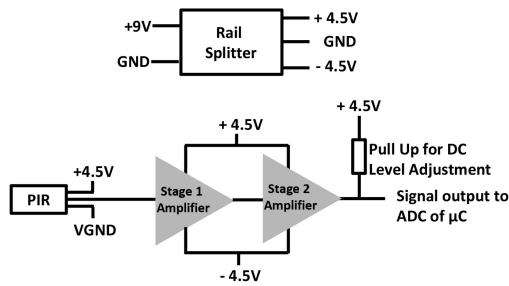


Fig. 6. Two stage amplifier electronics for PIR Sensor.

The PIR sensor signal is a function of the relative temperature difference between the moving object and its background (see (1)). The larger the temperature difference the larger will be the amplitude of the PIR sensor output and vice versa. Thus, a fixed gain cannot be used in a practical setting where the background temperature varies

throughout the day. To address this limitation one could measure the ambient temperature and adjust the gain of the potentiometers appropriately.

In order to avoid the cumbersome and time-consuming task of manually adjusting the potentiometers, we replace them with digital potentiometers whose resistance can be adjusted using a micro-controller (Fig. 7). An inter-integrated circuit (I2C) driver is used in conjunction with an I2C multiplexer to program each amplifier stage. We plan to utilize this circuit in conjunction with an ambient temperature sensor for automatic gain adjustment in future experiments.

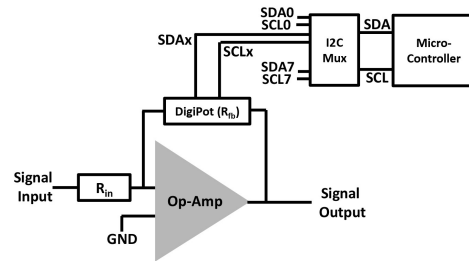


Fig. 7. Digital potentiometer for automatic gain control.

D. Operating Range of the STP

The STP is required to have the ability to distinguish between human and animal over a range of distances. A side view of the FoV of the STP is shown in Fig. 8. The inherent sensitivity of the PIR sensors as well as the divergent nature of the beams, making up the FoV, limit the operating range of the STP. The operating range of the STP developed here is 5-10m. At distances smaller than 5m, a small animal such as a dog will pass below all 4 beams *A, B, C, D* and hence will travel undetected as can be seen from Fig. 8. At ranges beyond 10m, the sensitivity of the sensors employed is not sufficient to guarantee detection with the required accuracy.

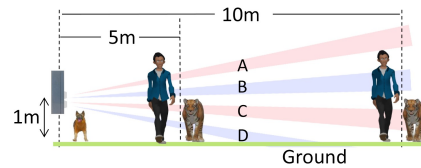


Fig. 8. The effect of diverging nature of the VPA.

IV. DATA COLLECTION

A key step in supervised machine learning is data collection. Supervised classification algorithms require labelled data from which the machine learns the classification model. The 3 classes of interest here are humans, animals and clutter. In general, data collection in the case of animals, particularly wild animals, is both challenging as well as time consuming. We collected dog-intrusion data at a dog-trainer facility in Bengaluru. Data corresponding to tiger, leopard and wolf intrusions were collected at the Bannerghatta Biological Park (BBP). Data corresponding to human intruder motion as well as clutter were gathered on the forested campus of the Indian Institute of Science. The collected data corresponded to straight-line motion at a variety of typically observed speeds and angles of inclination θ (see Fig. 9(a)) at various distances within the desired operating range of 5-10m.

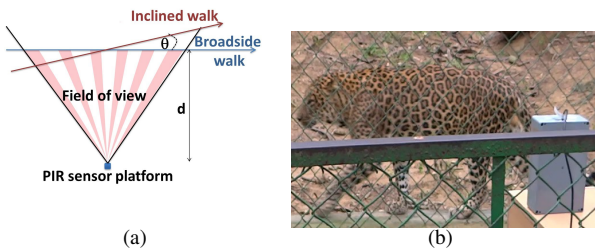


Fig. 9. (a) The angle of inclination θ of an intruder path relative to broadside walk is illustrated here. (b) One of the settings in which data were collected in the Bannerghatta Biological Park. The STP collecting data is visible in the foreground to the right.

V. ASPIRE: ANIMATION-BASED SIMULATION TOOL FOR PASSIVE INFRA-RED SENSOR

Given the difficulty noted in Section IV in gathering data associated to animal motion, an Animation-based Simulation tool for Passive Infra-Red sEnsor (ASPIRE) was developed to simulate data corresponding not only to animal motion, but also human motion and clutter as well. Animated 3D models of the intruder were developed using the popular animation software Blender. The 3D model consists of a collection of triangles that are arranged in the form of a mesh that approximates the outer surface of the intruder.

The key intermediate step in determining the signal resulting from motion of the 3D model across the FoV of the STP is to find the area of the 3D mesh when projected onto the VPA of

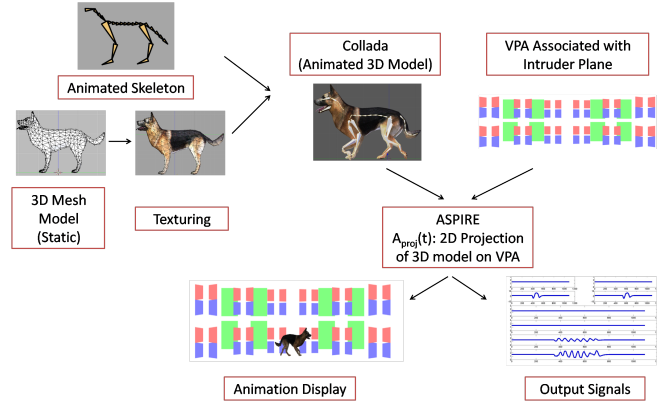


Fig. 10. ASPIRE block diagram to obtain the simulated PIR signal.

the STP. By VPA here, we mean the VPA that is associated with the vertical plane along which the intruder moves. The area of projection of the 3D mesh can in turn be determined by projecting all triangles in the mesh model onto the VPA and computing the area of the polygon obtained by taking the union of all these projected triangles.

To simplify computation, in place of actual area computation, what is done in practice is to divide the VPA into a very large number of tiny squares. The area is then to a good approximation equal to be the sum of the areas of all squares that have non-empty intersection with the projected 3D mesh. This is illustrated in Figs. 11(a) and 11(b). This approach is along the lines of the approach employed in computer graphics for rendering a scene [13].

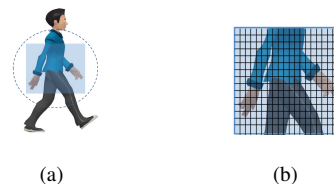


Fig. 11. Calculating the area of the intruder when projected onto the VPA.

Animation techniques have been used previously to simulate waveforms in conjunction with doppler sensing for the purposes of detection and classification of different types of human motion [14]. In that paper, the authors use Bio-Vision Hierarchy (BVH) files to simulate the motion of a human being as opposed to the more sophisticated Collada file format that we developed using Blender software.

VI. CHIRPLET-BASED MODEL FOR INTRUDER SIGNAL

In the classification algorithm that is discussed in Section VIII, we exploit the simple-but-useful observation, made to our knowledge for the first time here, that intruder signals are well modeled using a chirp. More specifically, the signals generated by the intruder moving across A, B, C, D arrays of the VPA exhibit chirp.

The chirp phenomenon is explained in Fig. 12. This figure presents a top view of the virtual beams generated by employing a multi-lens in conjunction with a PIR sensor. Consider an intruder moving along a circular path at uniform speed. In this case, the size of the virtual pixels encountered and the gaps between two consecutive pixels of the VPA will be equal throughout the duration of intruder motion. As a result, the response of the PIR sensor will resemble a periodic sinusoidal signal. In the case of intruder motion from left to right along the straight-line path shown in Fig. 12, the size of the virtual pixels and gaps between two successive pixels of the VPA initially decreases until the intruder reaches the point of closest approach and thereafter increases. Thus, an intruder moving at a uniform speed along such a straight-line path will generate a signal comprising of an up-chirp followed by a down-chirp as illustrated at the top of Fig. 12. The extent and nature of the chirp will depend upon the angle θ of inclination of the intruder path. Clearly, in the case of oscillatory motion corresponding to clutter, no such chirp will be present. Figs. 13(a) and 13(b) show signals of intruder and clutter events, respectively.

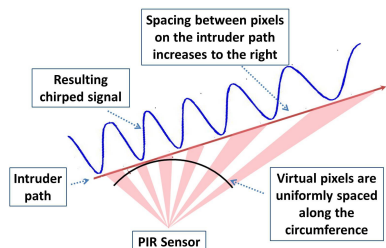


Fig. 12. Explaining the chirped signal that arises from intruder motion along a straight line at uniform velocity.

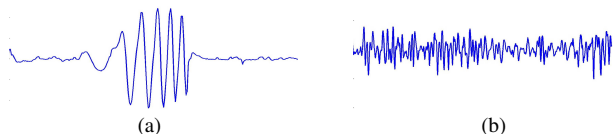


Fig. 13. Illustrating intruder and clutter signals.

A. Intruder Detection via Chirplet Decomposition

Our decomposition of the signal waveform as a sum of chirplets makes use of complex-exponential representation of elemental chirped signals in the form:

$$x(n; m, \omega, c, d) = (2\pi d^2)^{-\frac{1}{4}} \exp \left\{ - \left(\frac{n-m}{2d} \right)^2 \right\} \times \exp \left\{ j\omega(n-m) + j\frac{c}{2}(n-m)^2 \right\}, \quad (3)$$

where, m , ω , c and d are the parameters of the chirp signal representing the location in time, location in frequency, chirp rate and duration, respectively.

As a first step, we pass on from the real intruder signal $s(n)$ to its complex, analytic representation $s_a(n) = (s(n) + j\hat{s}(n))$, where $\hat{s}(n)$ is the Hilbert transform of $s(n)$. We next decompose $s_a(n)$ as the weighted sum of q chirplets

$$s_a(n) = \sum_{i=1}^q a_i e^{j\phi_i} x_i(n; m_i, \omega_i, c_i, d_i), \quad (4)$$

where, each $x_i(n)$ is given by an expression as in (3).

Next, maximum likelihood estimates of the parameters a , m , ω , c and d of each chirplet are found using the method in [15]. The intruder signals turn out to be well approximated by the sum of three chirplets. The chirplet decomposition and subsequent reconstruction of an intruder and clutter signal associated to sensors A and B are shown in Fig. 14.

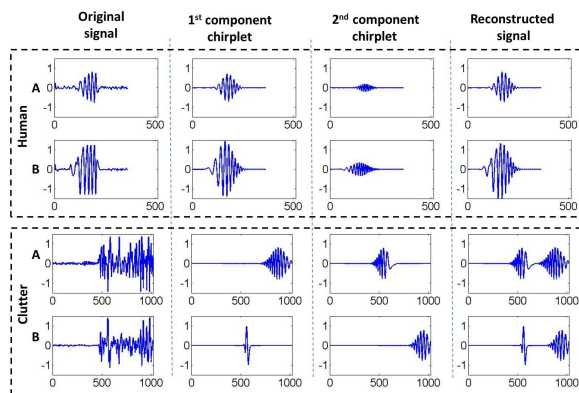


Fig. 14. Chirplet decomposition of the signals associated to sensors A and B in the case of both intruder motion as well as clutter are shown here. For the sake of clarity, only two components chirplets are shown.

Note that the reconstructed signal is close to that of the

original signal in the case of an intruder signal and this is not true in the case of signal arising from clutter. What is fed to the SVM, however, are the parameters corresponding to this 3-chirplet decomposition. As will be seen in Section VIII, this approach resulted in high classification accuracy for the data sets collected. Some justification for this approach can be seen from the fact that in the chirplet decomposition associated to clutter, the times of arrival m_i , of the different chirplet components, are well separated in time unlike in the case of an intruder signal, where the signals arrive synchronously. Also in terms of chirplet signal duration d_i , the different chirplets can have time durations that are very different, again unlike in the case of an intruder signal, where the time durations of the different chirplet components are very close to one another.

VII. OTHER FEATURES USED IN CLASSIFICATION

Key components of the feature vector used for classification were the parameters obtained from chirplet decomposition. Other important features employed relate to cross-correlation between signals obtained from sensors L_1, L_2, R_1, R_2 and the energy of signals from all 8 sensors as explained below.

A. Features Related to Signal Cross-Correlation

When an intruder moves say from left to right, the signals generated by sensors L_1, R_1 are slightly delayed and time-scaled versions of each other. A similar statement is true in the case of signals generated by sensors L_2, R_2 . As a result, these signals will be highly correlated. Clutter generated by vegetation whose motion is oscillatory as opposed to translational will be unlikely to exhibit high correlation.

The precise quantity relating to signal correlation employed as part of the feature vector is the maximum cross-correlation parameter ρ_{\max} corresponding to signals s_{L_i}, s_{R_i} generated by sensors $L_i, R_i, i = 1, 2$ and given by:

$$\rho_{\max} = \max_k \sum_n \sum_i \frac{s_{L_i}(n+k)s_{R_i}(n)}{\sqrt{(E_{L_1} + E_{L_2})(E_{R_1} + E_{R_2})}}, \quad (5)$$

where, $E_{L_i} = \sum_n s_{L_i}^2(n)$ and $E_{R_i} = \sum_n s_{R_i}^2(n)$ for $i = 1, 2$.

Histogram plots of ρ_{\max} observed for a large collection of events obtained both through real-world data collection and

simulation by ASPIRE are shown in Figs. 15(a) and 15(b), respectively. Note that in both data sets, ρ_{\max} tends to be high for intruder motion and small in the case of vegetative motion. The differences between the two plots can be attributed in part, to the fact that the simulation data were generated using a smaller number of shrubs (to keep the complexity of simulation manageable) than were encountered in the real world. In addition, animal motion in the real world tended to take place at a slower speed (at larger distances) than could be reliably measured by the STP.

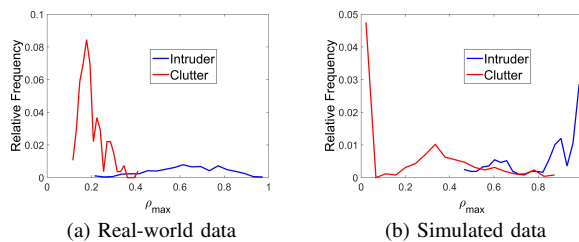


Fig. 15. Correlation histograms for real-world and simulated data.

B. Signal-Energy-Based Classification

Much effort went into designing the STP to endow it with a good spatial resolution. As can be seen from the data in Table II, it is possible to obtain some indication of the nature of the intruder and the intruder's relative distance simply by examining the energy of the signals generated in sensors A, B, C, D .

In the table, a 0 or 1 entry indicates that the energy received by the particular sensor lies below or above a certain preset threshold, respectively. For example, a human intruder will typically trigger signals in all four sensors A, B, C, D , whereas an animal intrusion will most often trigger signals in sensors C, D . If only sensors A, B register signals, this is very likely indicative of clutter motion. Other inferences that can be drawn, also appear in the table. In terms of implementation however, the energy from all 8 sensors are fed as a feature vector to an SVM. An important advantage is the relative ease of extracting energy levels and hence the use of such features in classification is attractive from the standpoint of implementation on a mote that has limited computational capability.

TABLE II
INFERENCE DRAWN BASED ON COMBINATION OF SENSORS A, B, C, D
THAT ARE TRIGGERED.

Sensor				Signal is indicative of
A	B	C	D	
0	0	0	1	short animal at 5 m
0	0	1	0	animal at 10 m
0	0	1	1	tall animal at 5 m
0	1	1	0	human at 10 m
0	1	1	1	short human at 5 m
1	1	1	1	human at 5 m
(all other combinations)				clutter or else, combination unlikely

VIII. CLASSIFICATION ALGORITHMS AND EXPERIMENTAL RESULTS

A. Database Description

Real-world and simulated databases were prepared. Each database covered a large number of events corresponding to either human or animal intrusion or else, clutter. Each event corresponded to a collection of (8×1024) samples from the 8 sensors with samples spaced 50 msec apart and hence corresponding to a time duration of approximately 50 secs. The break-up of the databases corresponding to the different event classes is shown in Table III. For each database, we used k-fold cross validation with 5 folds.⁵

B. Classification Algorithms

In the three-way classification considered here, there were three feature vectors employed which we will refer to as:

- $E_8 \Leftrightarrow$ the energy recorded by all 8 sensors ,
- $\rho_{\max} \Leftrightarrow$ the maximum correlation parameter,
- $C_{60} \Leftrightarrow$ the collection of 60 chirplet parameters.

The dimension of the feature vector C_{60} is given by

$$(5 \text{ parameters per chirplet}) \times (3 \text{ chirplets per sensor signal}) \\ \times (4 \text{ sensor signals}) = \text{total of 60 parameters.}$$

⁵The results presented in our previous paper [6] used the holdout method for cross-validation and a smaller range for the parameter C compared to what is employed in this paper. The parameter C is used in the SVM to control the trade-off between margin and allowed training errors.

TABLE III
EVENT DISTRIBUTION WITHIN THE DATABASE.

Real-World Data			
Human	Animal	Clutter	Total
209	151	134	494
Simulated Data			
Human	Animal	Clutter	Total
210	186	272	668

In terms of machine learning algorithm, we uniformly relied upon SVM. We will use $SVM(E_8)$ and $SVM(E_8 \cup \rho_{\max})$ to denote SVM-based classification algorithms that employed E_8 and $(E_8 \cup \rho_{\max})$ as their respective feature vectors, etc. We employed a 2-step classification algorithm. In the first step, we distinguished between intruder and clutter and in the next step we distinguish between human and animal intruder.

1) *Distinguishing Between Intruder and Clutter:* This turned out to be the more challenging aspect of classification. Here, we tried out several possible choices of features (see Fig. 16) and the corresponding classification results can be found tabulated in Tables IV and V. We present results that represent the minimum and average accuracies attained. Our findings can be summarized as follows:

- (a) **Improvement due to correlation parameter ρ_{\max} :**
The performance of $SVM(E_8 \cup \rho_{\max})$ was noticeably better than that of $SVM(E_8)$ showing the parameter ρ_{\max} to be relevant in this context.
- (b) **Efficacy of Chirplet Parameter set C_{60} :**
 - Interestingly, $SVM(C_{60})$ significantly outperformed $SVM(E_8 \cup \rho_{\max})$ despite the fact that the former only makes use of data from sensors A, B, C, D .
 - In the context of C_{60} data, both ρ_{\max} and E_8 turned out to improve performance only marginally. Based upon these results, the decision was made to select the classifier based only on C_{60} as the feature vector.
- (c) **Animation as a useful tool for algorithm testing:**
The relative performance of the various algorithms on real-world and simulated data was very similar, that suggests animation is a very useful tool in this setting. The performance of $SVM(E_8)$ on simulated data was lower compared to the performance on real-world data as some of the clutter events generated by ASPIRE were similar to intruder events. Such events were not present in the real-world database.

TABLE IV
INTRUDER VERSUS CLUTTER - ACCURACY WITH REAL-WORLD DATA

Features			Minimum Accuracy %			Average Accuracy %		
E_8	ρ_{\max}	C_{60}	Clutter	Intruder	Total	Clutter	Intruder	Total
✓			96.3	94.2	94.8	96.3	97.4	97.1
✓	✓		96.3	95.6	95.8	97.8	97.4	97.5
		✓	100	98.6	99.0	98.5	99.7	99.4

TABLE V
INTRUDER VERSUS CLUTTER - ACCURACY WITH SIMULATED DATA

Features			Minimum Accuracy %			Average Accuracy %		
E_8	ρ_{\max}	C_{60}	Clutter	Intruder	Total	Clutter	Intruder	Total
✓			87.0	88.6	88.0	92.6	92.9	92.8
✓	✓		87.0	96.2	92.5	94.1	95.0	94.6
		✓	98.2	97.5	97.8	99.3	99.2	99.3

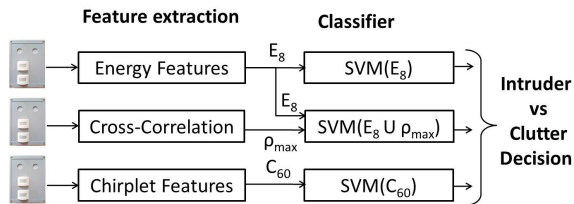


Fig. 16. Intruder vs clutter classification using energy, correlation and chirplet based feature vector.

2) *Distinguishing Between Human and Animal*: In the second and final classification step, in order to distinguish between a human and animal, we simply fed the output of E_8 to an SVM that carried out the binary classification. The spatial-resolution of the STP served us in good stead here, resulting in high-accuracy decisions.

3) *Classification Algorithm Finally Selected*: Our 2-step classifier utilized the C_{60} feature vector for intruder vs clutter classification. Upon detecting the presence of an intruder, E_8 features were then used to classify between human and animal in the second step (see Fig. 17).

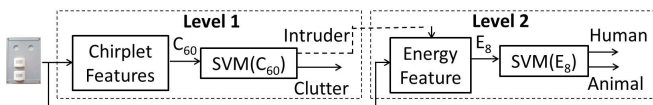


Fig. 17. Final 2-step classifier that utilizes C_{60} and E_8 features.

The minimum and average accuracies obtained on real-world and simulated data are shown in Table VI.

TABLE VI
OVERALL CLASSIFICATION ACCURACY - 2-STEP CLASSIFIER ON REAL-WORLD AND SIMULATED DATA

	Real World Data		Simulated Data	
	Minimum Accuracy	Average Accuracy	Minimum Accuracy	Average Accuracy
Clutter	92.3 %	97.8 %	98.1 %	99.6 %
Intruder	100 %	98.6 %	98.7 %	99.2 %
Human	97.4 %	98.5 %	100.0 %	100.0 %
Animal	96.7 %	98.6 %	100.0 %	100.0 %
Overall	95.8 %	97.3 %	98.5 %	99.4 %

IX. CONCLUSIONS AND FUTURE WORK

The paper presents the design of a PIR STP that featured the use of (a) an array of PIR-sensors and lens combinations to endow the platform with the spatial resolution needed to distinguish between human, animal and vegetative clutter, (b) ASPIRE, a simulation tool that we developed that allowed us to judge the efficacy of various approaches to classification without the need for time consuming and challenging animal-motion data collection and (c) the modeling of an intruder signal as a waveform exhibiting chirp that

was effective in discriminating between intruder motion and clutter. The overall average classification accuracy was found to be quite high, over 97%.

The classification algorithm was carried out offline on a laptop as the complexity of extracting the 60 chirplet parameters exceeds the computational capabilities of the processor on the mote. It is planned as future work, to identify the key parameters among the 60 chirplet parameters employed for classification here with the aim of significantly reducing the complexity of the classification algorithm to the point where it can be implemented on a mote.

X. ACKNOWLEDGMENT

We would like to acknowledge the help extended to us by the Executive Director and Staff at Bannerghatta Biological Park and dog trainer at Dog Guru for animal data collection.

REFERENCES

- [1] A. Arora *et al.*, "Exscal: Elements of an extreme scale wireless sensor network," in *Proc. IEEE Int. Conf. Embedded and Real-Time Computing Syst. and Applicat.*, 2005, pp. 102–108.
 - [2] L. Gu *et al.*, "Lightweight detection and classification for wireless sensor networks in realistic environments," in *Proc. Int. Conf. on Embedded Networked Sensor Syst.* ACM, 2005, pp. 205–217.
 - [3] SmartDetectTeam, "Wireless sensor networks for human intruder detection," *Journal of the Indian Institute of Science, Special Issue on Advances in Elect. Sci.*, vol. 90, no. 3, pp. 347–380, 2010.
 - [4] S. G. Hong, N. S. Kim, and W. W. Kim, "Reduction of false alarm signals for PIR sensor in realistic outdoor surveillance," *J. ETRI*, vol. 35, no. 1, pp. 80–88, 2013.
 - [5] E. L. Jacobs, S. Chari, C. Halford, and H. McClellan, "Pyroelectric sensors and classification algorithms for border/perimeter security," in *Proc. SPIE Europe Security+ Defence*, 2009, pp. 74 810P–74 810P.
 - [6] R. Upadrashta *et al.*, "An animation-and-chirplet based approach to intruder classification using pir sensing," in *Proc. IEEE Int. Conf. Intell. Sensors, Sensor Networks and Inform. Process.*, 2015, pp. 1–6.
 - [7] J. Zhao, W. Gong, Y. Tang, and W. Li, "Emd-based symbolic dynamic analysis for the recognition of human and nonhuman pyroelectric infrared signals," *J.Sensors*, vol. 16, no. 1, p. 126, 2016.
 - [8] S. B. Lang, "Pyroelectricity: from ancient curiosity to modern imaging tool," *J. Physics Today*, vol. 58, no. 8, pp. 31–36, 2005.
 - [9] R. Whatmore, "Pyroelectric devices and materials," *J. Rep. Prog. Phys.*, vol. 49, no. 12, p. 1335, 1986.
 - [10] F. A. S. Military Analysis Network, "Infrared propagation and detection," [accessed 9-June-2015]. [Online]. Available: http://fas.org/man/dod-101/navy/docs/es310/IR_prop/IR_prop.htm
 - [11] A. Hossain and M. H. Rashid, "Pyroelectric detectors and their applications," *IEEE Trans. Ind. Appl.*, vol. 27, pp. 824–829, 1991.
 - [12] A. Chattopadhyay *et al.*, "PIR-based wsn for outdoor deployment," in *Proc. IEEE Int. Conf. on Wireless Commun. and Sensor Networks*, 2012.
 - [13] T. Theoharis, G. Papaioannou, and E.-A. Karabassi, "The magic of the z-buffer: A survey," in *Proc. Int. Conf. Comput. Graph., Visualization and Comput. Vision*, 2001, pp. 379–386.
 - [14] S. S. Ram and H. Ling, "Simulation of human microdopplers using computer animation data," in *Proc. IEEE Radar Conf.*, 2008, pp. 1–6.
 - [15] J. C. O'neill, P. Flandrin, and W. C. Karl, "Sparse representations with chirplets via maximum likelihood estimation," 2001.
- Raviteja Upadrashta** received the M.S. in Electrical Engineering from IIT Madras, Chennai in 2008. He is currently pursuing his Ph. D. in Department of Electrical and Communication Engineering at IISc, Bengaluru.
- Tarun Choubisa** received the M.Tech. in Digital Signal Processing from IIT Guwahati in 2010. He is currently pursuing his Ph. D. in Department of Electrical and Communication Engineering at IISc, Bengaluru.
- A. Praneeth(M'09)** received B.E. in Electronics and Communication from PES College of Engineering in 2003 and M. E. (Telecom) from IISc in 2015. He is currently working with DRDO.
- Tony G.** received B. Tech. in Electrical and Electronics from NIT Calicut in 2013 and M. E. (Signal Processing) from IISc Bangalore in 2015. He is currently working in Flytxt Trivandrum as R & D Lead Data Science.
- V. S. Aswath** received B. Tech. from department of electrical engineering from NIT Calicut in 2011, and M. E. degree in Signal processing from IISc in 2013. Currently employed with Broadcom India Research.
- P. Vijay Kumar (S'80-M'82-SM'01-F'02)** received his Ph.D. from USC in 1983 in Electrical Engg. From 1983 to 2003 he was on the faculty of the EE-Systems Department at USC. Since 2003, he has been on the faculty of IISc, Bengaluru. He also holds the position of Adjunct Research Professor at USC. His current research interests include codes for distributed storage and intrusion-detection algorithms for WSNs. He is an ISI highly cited author and a Fellow of the Indian National Academy of Engg. He is also co-recipient of the 1995 IEEE Information Theory Society Prize-Paper award, a Best-Paper award at the DCOSS 2008 conference on sensor networks and the IEEE Data Storage Best-Paper Award of 2011/2012. A pseudo-random sequence family designed in a 1996 paper co-authored by him now forms the short scrambling code of the 3G WCDMA cellular standard. He received the USC School of Engineering Senior Research Award in 1994 and the Rustum Choksi Award for Excellence in Research in Engg. in 2013 at IISc. He has been on the Board of Governors of the IEEE Information Theory Society since 2013.
- Sripad Kowshik** received B.E. in Electronics and Communication from Sri Venkateshwara College of Engg. in 2012. He is currently pursuing M.S. in Electrical Engg. and Computer Science at University of California, Irvine.
- Hari Prasad Gokul R** received the B.E. degree in Electronics and Communications Engineering from PSG College of Technology (Anna University), Coimbatore, in 2013 and is currently a Project Assistant with the Department of Electronic Systems Engineering, IISc, Bangalore, India.
- Prabhakar Venkata** received M.Sc. (Engg.) from IISc, Bengaluru and PhD from TUDelft, Netherlands. He works as Senior Scientific Officer in the Department of Electronic Systems Engg, IISc, Bengaluru. His area of work is in Networked Embedded Systems. His research interest is in Energy Harvesting systems, Power Management Algorithms, Tactile IoT. The broad spectrum comprises of Modelling, Virtual Prototyping, System Building and Performance evaluation. His work in LED based communication won the best demo award in COMSNETS 2014. He is currently working on RFID localization algorithms, RF energy harvesting technologies in chip design and Indoor localization applications in healthcare and safety. The Zero Energy Networks laboratory (ZENLab) at IISc specializes in building ultra low power embedded boards and software stacks. The application areas are related to Smart Grids, Healthcare, Human Security and Agriculture.